Pergamon

Int. J. Heat Mass Transfer. Vol. 41, No. 1, pp. 147–158, 1998

Printed in Great Britain
0017–9310/98 $19.00+0.00

PII: S0017–9310(97)00065–3

Cluster motion and particle-convective heat transfer at the wall of a circulating fluidized bed

PETER D. NOYMER and LEON R. GLICKSMAN†

Department of Mechanical Engineering, Massachusetts Institute of Technology, Cambridge, MA 02139, U.S.A.

(*Received* 17 *May* 1996 *and in final form* 19 *February* 1997)

Abstract—A new technique has been developed to observe and measure the hydrodynamic properties of solid particles flowing at the wall of a fluidized bed. This technique is called 'thermal image velocimetry' or TIV. The TIV technique involves heating the clusters of particles that are at the wall and using their radiant emission to distinguish them from the rest of the bed, with an infrared camera as the detection device. The current setup is in a cold scale-model circulating fluidized bed with a riser that has a 0.159 m square cross-section and is 2.44 m tall. The TIV test section is located on one wall in the upper half of the riser. The hydrodynamic properties that have been measured are the descent velocities of clusters of particles at the surface of a flat wall and the contact times of these clusters with the wall. The measured cluster velocities are between 0.9 and 1.2 m s^{-1}, apparently accelerating to the higher value near the end of their travel. These velocities appear to be independent of the operating conditions (solid and gas flow rates) in the bed, and the apparent acceleration can be shown to affect heat transfer from the clusters. The average contact times measured are around 0.4 s, and a probabilistic analysis shows that individual cluster–wall contact times are distributed according to a gamma probability function. This analysis also highlights the concept of a thermal development region for particle-convective heat transfer. © 1997 Elsevier Science Ltd.

INTRODUCTION

As circulating fluidized beds (CFBs) become more widely used as boilers, it becomes beneficial to understand the mechanisms of heat transfer from CFBs. A better understanding of these heat transfer mechanisms will allow for better designs and more efficient systems. The energy in a CFB is typically exchanged with water tubes that comprise the wall of the riser, so that the mechanisms for heat transfer can be described by the interactions between the bed material, the gas and the wall. In a core-annular flow regime, as seen in the upper portion of a CFB, the flow of bed material near the wall is predominantly downward in agglomerations of particles known as clusters [1, 2]. Other investigators have found clusters to have the following features: the characteristic size of a cluster is approximately 0.5–2.0 cm [3, 4]; a typical solid concentration in a cluster is approximately 10–30% [2, 5]; a typical descent velocity is between 0.5 and 2.0 m s^{-1} [3, 6]; and the typical shape projected at the wall is somewhat oval or elliptical [4].

Omitting the radiant heat transfer contribution (considering it to be additive), the heat transfer from the bed to the wall is typically modeled as a combination of convection from the upward-flowing gas and conduction from the downward-moving clusters, also called 'particle convection'. The following are aspects of the heat transfer model: the wall is either covered by gas or clusters, so that gas and particle convection are presumed to act in parallel on the same heat transfer surface [7]; particle convection consists of clusters exchanging energy via transient conduction with the wall [8], though imperfect contact results in an added thermal resistance [9]; and the gas-convective contribution can be reasonably estimated using correlations for single-phase gas flow [5]. As a result, the total convective heat transfer at the wall of a CFB is modeled using the following equation:

$$h_{\text{conv}} = (1-f)\cdot h_{\text{gas}} + f\cdot\left(R_{\text{contact}} + \sqrt{\frac{\pi t}{(k\rho c)_{\text{cluster}}}}\right)^{-1}. \quad (1)$$

A number of the heat transfer parameters in equation (1) are functions of the hydrodynamics in a CFB, such as: f, the fraction of the wall covered by clusters; R_{contact}, the contact resistance between the cluster and the wall; t, the time of contact between clusters and the wall; and k, ρ and c, the physical properties of the cluster, which are dependent on cluster porosity [10]. Since so much of equation (1) is based on hydrodynamic phenomena, the ability to observe, measure and predict these phenomena under various

† Author to whom correspondence should be addressed.

NOMENCLATURE

c	specific heat capacity [J kg^{-1} K]
C	arbitrary drag coefficient [units vary]
d_p	mean particle diameter [m]
D	bed diameter [m]
e	energy per unit area [J m^{-2}]
f	fraction of wall covered by clusters [—]
g	gravitational acceleration [m s^{-2}]
G_s	solid recirculation rate [kg m^{-2} s]
h	heat transfer coefficient [W m^{-2} K]
k	thermal conductivity [W m^{-1} K]
K	parameter for particle-convective heat transfer [—]
L	riser height [m]
M_c	mass of a cluster [kg]
$m(\tau)$	probability distribution of measured contact times [—]
n	parameter for gamma probability distribution [—]
Nu	Nusselt number [—]
$p(t)$	probability distribution of actual contact times [—]
P	bed pressure [atm]
R	thermal resistance [m^2 K W^{-1}]
t	time, actual contact time between cluster and wall [s]
T	bed temperature [K]
u_c	cluster velocity [m s^{-1}]
u_0	gas superficial velocity [m s^{-1}]
x	distance [m]
x_0	adiabatic starting distance for heat transfer surface [m].

Greek symbols

ε	volumetric void fraction [—]
η	dimensionless time [—]
η_{avg}	average dimensionless contact time [—]
ρ_g	gas density [kg m^{-3}]
ρ_s	solid density [kg m^{-3}]
τ	measured contact time between cluster and wall [s]
ζ	dimensionless distance [—]
ζ_0	dimensionless adiabatic starting distance [—].

operating conditions would allow for a better understanding and the ability to predict bed-to-wall heat transfer rates under various operating conditions.

In this work, we are interested in observing and measuring t, the cluster–wall contact time. Local cluster velocities have been measured, as discussed previously, and there have been reports of measurements of the length of contact between clusters and the wall [11, 12]. Typically, one might take the length measurement and divide by the velocity to calculate a contact time. However, there is no indication that the cluster velocity is constant for the entire contact length; in fact, it has been postulated that there is some acceleration to a terminal velocity, as with a body in gravitational free fall [13]. Furthermore, the length measurements reported either measure the contact length by cross-correlating heat transfer rates from probes that are relatively far apart [11] or they are inferred from heat transfer measurements by using the particle-convective heat transfer model in equation (1) [12]. None of these observations actually identify clusters as having remained at the wall, and it was with this in mind that a new technique was developed to measure cluster velocities and contact times between clusters and the wall. We call this technique 'thermal image velocimetry' or TIV, and it involves heating the clusters and using their radiant emission to detect their motion at the wall. The concepts behind TIV and its implementation in these experiments are discussed in the next section.

DESCRIPTION OF APPARATUS AND EXPERIMENTS

Scale-model CFB

All the experiments reported here were conducted in a cold scale-model CFB, which was originally built as a 1/4-scale model of a 2 MW_{th} combustor [14]. The riser is 2.44 m high with a square cross-section measuring 0.159 m on each side; the walls are made of clear polycarbonate plastic. Pressure taps along the riser wall allow for the measurement of differential pressures and the calculation of average solid concentrations in the riser. The riser has a sharp 90° exit at the top, and the solids are returned to the bottom of the bed via an aerated L-valve. Figure 1 shows a schematic of the scale-model CFB. The bed material is steel powder, with a material density of 6980 kg m^{-3} and a mean particle diameter of 69 μm. Using scale-up rules for CFBs [15], it can be shown that this allows for the simulation of a larger CFB combustor operating at atmospheric pressure. Table 1 gives the general specifications of the cold scale-model CFB and the hypothetical full-sized bed being simulated.

Experimental technique and equipment

The basic concept behind the TIV system is that heating the clusters at the wall alters their emission of thermal radiation, and thereby distinguishes them from the rest of the bed. With the appropriate detection device, such as an i.r. camera, properties of the

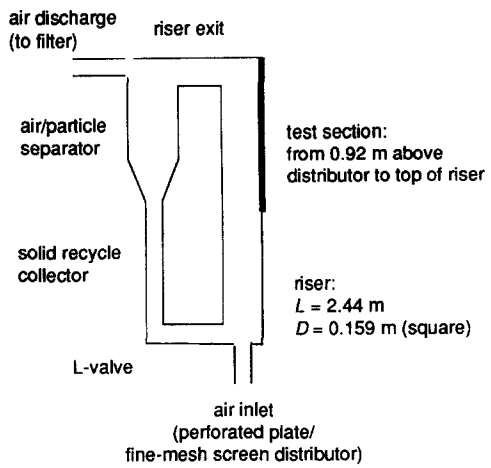

Fig. 1. Schematic for scale-model CFB.

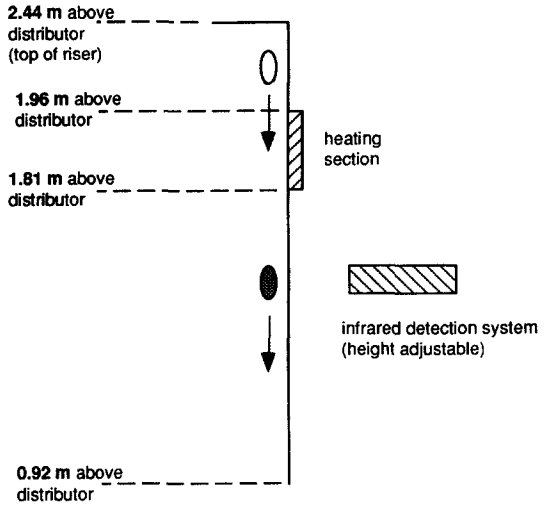

Fig. 2. Schematic for this TIV test section.

flowing clusters can be measured. TIV has several advantages, among them: it is a noninvasive method for marking the clusters and tracking their motion at the wall as TIV does not require any instrumentation in the flow path; it does not require the addition of tracer particles to the flow to enhance flow visualization, which is beneficial since such particles might affect the hydrodynamics in the riser; and the simple method of thermally marking the clusters does not require the bed material to be any special material itself (such as a photo-luminescent substance) which allows for the selection of a material which will yield similitude with any desired full-sized configuration. Furthermore, the thermal marking and tracking of clusters allows distinct advantages over conventional video systems: one can easily distinguish clusters at the wall from both material in the core of the CFB *and* new material deposited at the wall, which can be extremely difficult under normal operating conditions; and the location of the stationary heater provides a firm reference point from which to make measurements.

In general, a TIV system in a CFB requires a test section containing three items: a heater for the clusters; a system capable of detecting i.r. radiation; and a wall that is transparent to i.r. radiation. Figure 2 shows a schematic of a test section, as well as the relative positioning of each item within this CFB. The heater must be made flush with the wall of the CFB so that the flow of the solids and the gas remains undisturbed, since small roughness elements on the wall have been shown to disrupt the flow of clusters at the wall [16]. The heater will also need to have enough power to raise the temperature of the clusters such that they do not cool down to the ambient bed temperature before they reach the end of the test section.

When running the cold scale-model CFB, the temperatures of both the heated and unheated clusters are of the order of 300 K, so that most of the thermal radiation emitted is in wavelengths around 10 μm. Because of this, an i.r. camera is required to observe the flow of the marked clusters; we used the Model 600 Imaging Radiometer from Inframetrics, Inc. In addition, most types of glass and plastic materials used for walls of scale-model CFBs absorb all radiant energy at wavelengths above roughly 2 μm. Therefore, a special wall is required to allow for the transmission of the radiant signal from the solid material at the wall. For the wall, we used a sheet of low-density polyethylene. At a thickness of 0.5 mm, LDPE attenuates roughly half of the radiation at wavelengths of about 10 μm, which is the region of interest for room-temperature experiments. Since measuring the temperature of the clusters is not our primary concern, we need not be worried that some of the signal is being attenuated; we merely need to be able to detect the radiant signal to indicate the presence of a cluster. Figure 3 shows a more detailed schematic of the construction of the wall, including the grid used to support the LDPE wall. Figure 4 shows sample pictures of clusters from the i.r. camera; these are still frames captured from the video output. With the i.r. camera, higher temperatures show up whiter in color, so that the 'white' objects in Fig. 4 are actually the heated

Table 1. General specifications for scale-model and hypothetically scaled-up CFBs

Parameter	Scale-model	4:1 scale-up
L [m]	2.44	9.76
D [m]	0.159	0.636
Cross-section shape	square	square
T [K]	300	1100
P [atm]	1.0	1.0
ρ_g [kg m^{-3}]	1.2	0.33
ρ_s [kg m^{-3}]	6980	$\approx$2500
d_p [μm]	69	$\approx$230
Typical u_0 [m s^{-1}]	3	6
Typical G_s [kg m^{-2} s]	25	18

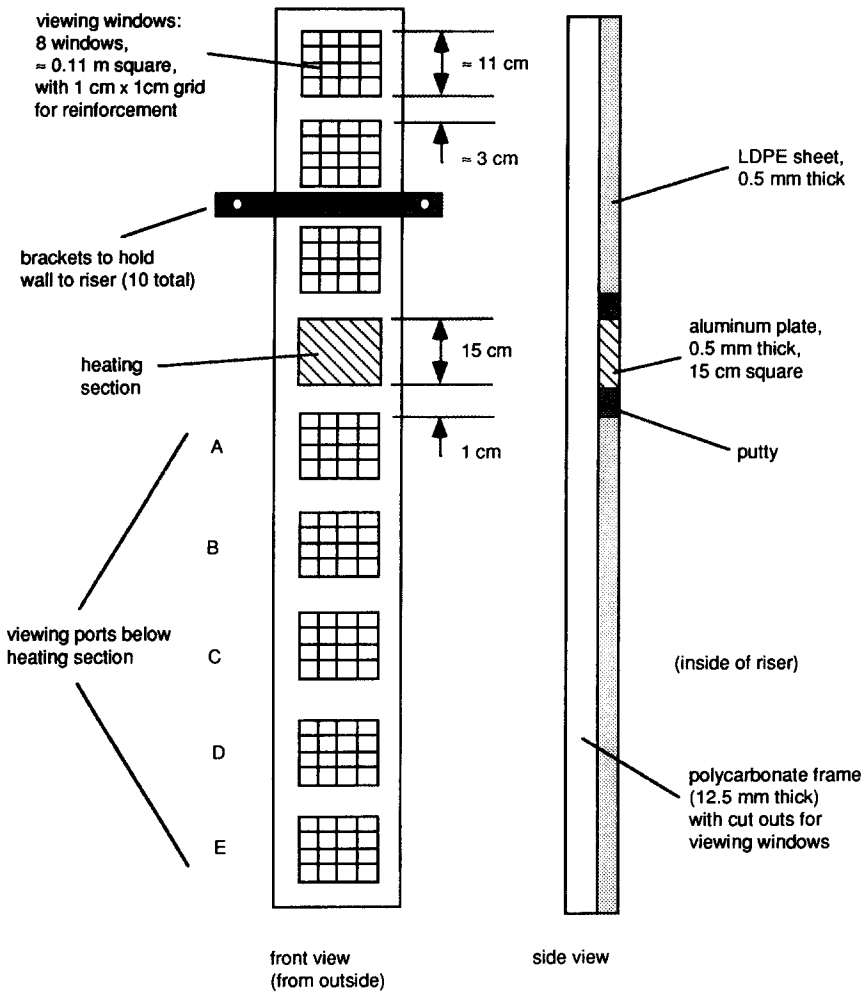

Fig. 3. Construction details for the wall in the TIV test section (not to scale).

clusters. The 'black' grid that appears is the grid supporting the LDPE, both of which are at ambient temperature.

It should be noted that the primary mode of heat transfer from the heater to the clusters near it is by conduction through the intervening gas layer, as described in equation (1). At the temperatures described, radiative transfer is negligible. Therefore, clusters of material that are distant from the wall will not have an observable increase in their temperature even if they can 'see' the heater surface. It should also be noted that clusters can easily be distinguished from the more dilute gas–solid mixture surrounding them. This is confirmed by the close agreement found between inspection of cluster motion using the i.r. camera and cluster motion using a conventional video camera.

Experimental operating conditions

The scale-model CFB was run at a total of eight different operating conditions for these experiments.

Table 2. Experimental operating conditions

Case #	Superficial velocity [m s^{-1}]	Solid recycle rate [kg m^{-2} s]	Average local cross-sectional solid conc.
1	2.3	9.3	0.25%
2	2.8	11	0.21%
3	2.8	19	0.46%
4	2.7	30	0.56%
5	3.3	18	0.24%
6	3.3	28	0.42%
7	3.6	25	0.28%
8	3.6	34	0.49%

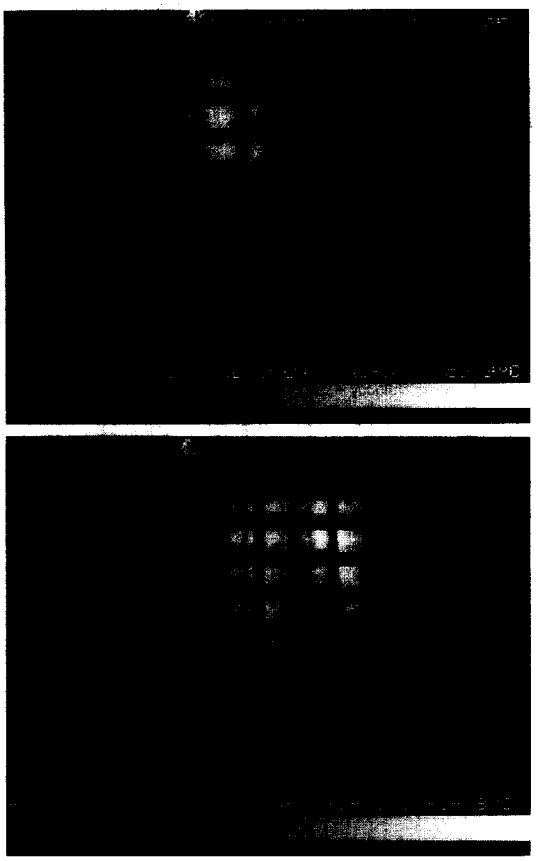

Fig. 4. Infrared images of heated clusters (white objects are heated clusters adjacent to wall).

The gas velocities and solid recycle rates were varied in order to understand the effect of operating conditions on the velocities and contact times being measured. Table 2 lists the different operating conditions, along with the average local solid concentrations in the TIV test section.

RESULTS—MEASUREMENTS OF CLUSTER VELOCITIES AT THE WALL

Overview

With viewing ports below the heating section (as shown in Fig. 3), the cluster velocities are measured by keeping the camera focused on a particular viewing port for some period of time. The camera samples images at 30 Hz, so that the number of frames it takes for a cluster to pass in and out of a viewing port indicates the time. Each viewing port has a known length, and dividing by the time for a cluster to pass through the field of view yields the velocity in that region. These velocities can be averaged for a number of clusters passing through that viewing port in the sampling time. Furthermore, there are five of the viewing ports below the heating section (also shown in Fig. 3), allowing for the measurement of any change in cluster velocities as they move along the wall. In a more sophisticated TIV system, two i.r. cameras could be used, allowing for cross-correlation techniques to be utilized in the measurement of cluster velocities.

Cluster velocities—measurements

Table 3 lists the velocities in each viewing port for each operating condition. These velocities are based on an average of about 10 or 12 clusters observed in each window for each operating condition. Figure 5(a) shows the variation of cluster velocity with time at the wall below the heating section, where the velocity history is used to convert distance along the wall to time at the wall. It should be noted that there is a fairly large amount of error in the velocity measurements, roughly $\pm 30\%$ for each measurement of average velocity. The bulk of the error results from the relatively low sampling rate of the camera. Since the viewing ports are about 0.11 m long, and the clusters move at about 1 m s^{-1}, it only takes about three frames for a cluster to pass through the field of view. The absolute error can be estimated at half a frame, resulting in a precision error that is about 20% of the measured value. The additional 10% results from applying 90% confidence limits to the statistical distribution of the data.

Cluster velocities—discussion

Several conclusions emerge from the measurement of the cluster velocities. The first is qualitative: that the direction of the motion of clusters was observed to be downward. These results are not explicitly seen in any of the tables or figures; however, some i.r. video segments were taken in the viewing port immediately above the heating section. In these videos, no cluster motion was observed. This observation (or lack thereof) was made under three different sets of operating conditions that are representative of the eight sets listed previously: $u_0 = 3.0$ m s^{-1} and $G_s = 10$ kg m^{-2}

Table 3. Measurements of average cluster descent velocities

Viewing port	Distance below heater [m]	Average cluster velocity [m s^{-1}] by case (see Table 2 for operating conditions)							
		1	2	3	4	5	6	7	8
A	0.067	0.81	0.98	0.88	0.81	0.93	0.83	0.90	0.93
B	0.205	1.14	1.14	1.00	1.14	1.14	1.14	1.14	1.14
C	0.338	1.30	1.27	1.06	1.07	1.08	1.10	1.06	0.98
D	0.470	1.33	1.33	1.14	1.07	1.15	1.30	1.21	1.19
E	0.610	1.23	1.20	1.33	0.97	1.16	1.30	1.25	1.04

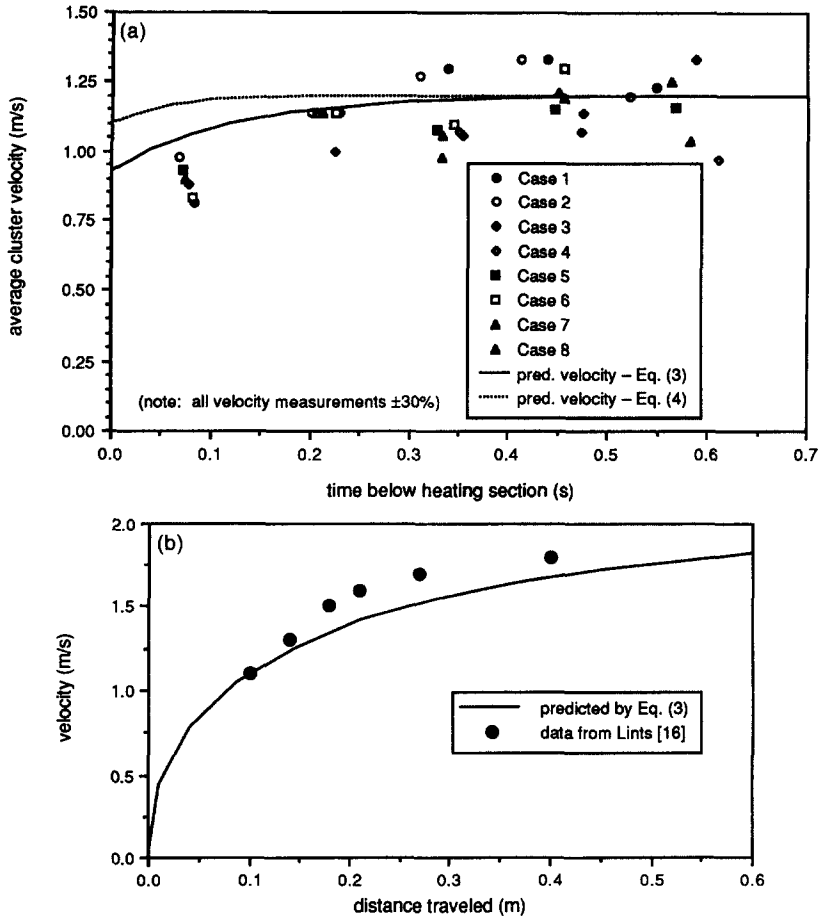

Fig. 5(a). Average cluster velocity vs time below heating section: measurements and predictions. (b). Cluster drag model applied to data of Lints [16].

s, $u_0 = 2.9$ m s^{-1} and $G_s = 20$ kg m^{-2} s, and $u_0 = 2.6$ m s^{-1} and $G_s = 10$ kg m^{-2} s. The downward motion of the clusters is consistent with the core–annular flow behavior in CFBs, as discussed previously.

We also observed that the velocity of the clusters increases the longer they travel at the wall. The clusters have been at the wall for some period of time prior to passing the end of the heating section, so that any initial velocity or acceleration cannot be observed. However, acceleration is still observed after heating, and this acceleration seems to taper off the longer the clusters are falling, indicating that the observed phenomenon is similar to the free fall of a body to a terminal velocity in a gravitational field. As discussed earlier, the existence of this phenomenon at the wall of a CFB has been postulated [13] and observed with particles descending in an empty tube with upward gas flow [16], but never observed in a fully-operational CFB. One consequence of this is that since cluster descent velocities are not constant, it might be inaccurate to state that t, the time of contact between the cluster and the wall, can be calculated by simply dividing some contact length by some cluster velocity.

It is also apparent that the velocities of the clusters are independent of the operating conditions in the CFB. For the eight different sets of gas velocities and solid recycle rates (and resultant solids concentrations), there is very little difference in the measured cluster velocities at a given point below the heater. Whatever variation is observed from case to case certainly falls within the range of the experimental uncertainty. Furthermore, the phenomenon of acceleration, with the velocity approaching a constant terminal velocity, is also observed in every case, and this terminal velocity is roughly constant at about 1.2 m s^{-1}. This value is comparable with those reported by other investigators, where cluster velocities have been reported to be between 0.3 and 2.0 m s^{-1} and independent of operating conditions in a given CFB [3, 6].

Finally, we can consider two models for the drag on a cluster in order to calculate and predict its velocity history. In one model, the drag force is linearly proportional to the velocity, resulting in the following equation of motion for the cluster:

$$M_c \frac{du}{dt} = M_c g - C_1 u \tag{2}$$

where u is the descent velocity of the cluster and C_1

is the 'drag coefficient'. Solving equation (2) for the conditions $u(0) = 0$ and $u(\infty) = u_c$, we find:

$$u(t) = u_c\left[1-\exp\left(\frac{-gt}{u_c}\right)\right]. \quad (3)$$

This solution might be typical when most of the drag on the cluster results from flow through the porous cluster or from a shear interaction with the adjacent wall. In the other model, the drag force is proportional to the square of the velocity, as with flow around a solid body at a high Reynolds number. Based on cluster sizes and velocities discussed previously, characteristic Reynolds numbers might be between 100 and 1000, which is sufficiently high to consider inertial forces in flow over a blunt body. This model results in the following equation of motion for the cluster:

$$M_c\frac{du}{dt} = M_c g - C_2 u^2 \quad (4)$$

where C_2 is the drag coefficient for this case. Equation (4) is difficult to solve analytically, but it can be solved numerically. The solution to this and equation (3) are superimposed on the measurements of cluster velocities in Fig. 5(a). The zero-point on Fig. 5(a) is assumed to correspond to $t = 0.2$ s for equations (3) and (4), since passing the heating section nominally represents half of the travel time for a cluster (and the total travel time ≈ 0.4 s, as discussed later). By inspection, it appears that the model for a drag force that is linearly proportional to the velocity characterizes the data best. For comparison, the data of Lints [16] is shown in Fig. 5(b) along with the velocity history predicted by equation (3).

RESULTS—MEASUREMENTS OF CLUSTER-WALL CONTACT TIMES

Overview

Similar to the measurement of cluster velocities, the i.r. camera was kept focused on each viewing port (see again Fig. 3) for a certain period of time. By analyzing the resulting videotape in slow motion, the average number of clusters passing by a particular viewing port in a given period of time were measured; we call this the "passing frequency" of clusters, where clusters have been defined previously. Since the TIV technique is still developmental, there is room for improvement over the current manual methods for data reduction. To allow for slightly greater resolution of the passing frequencies, the top and bottom halves of the first viewing port were analyzed separately when replaying the videotape. To retain consistency with the nomenclature thus far, the two halves of viewing port A can be referred to as A1 and A2 for the top and bottom halves, respectively.

The viewing ports are located at fixed distances below the heated plate; therefore, the passing frequency in each viewing port actually represents the passing frequency as a function of the distance traveled after heating. Since the velocity history of the clusters below the heated plate is known for each operating condition (these results are presented in the previous section), the passing frequency is also known as a function of the travel time below the heated plate. If normalized, the passing frequency can be thought of as a probability function for observing a cluster a certain time after heating. With that, the rate of change of the passing frequency, or the 'shedding function,' is the probability function for a cluster disappearing from the wall a certain time after heating. Restated, this is the probability that a cluster remains in contact with the wall certain time after heating, which is precisely the information we seek. A probabilistic analysis shows that the total contact time at the wall is about twice the contact time after heating.

When a cluster disappears from view, or when a change in passing frequency is measured, it can be assumed that the cluster was shed from the wall. Since the detection of clusters depend on their temperature, it may be possible that the disappearance of clusters results from cooling or even perhaps from clusters mixing. A simple analysis can show that the heater has enough power to sufficiently raise the temperature the clusters such that they can still be observed by the end of the entire test section. Regarding mixing, observation with conventional video in this CFB show that this is not an issue.

Cluster–wall contact times—measurements

The cluster–wall contact times were measured under the same operating conditions as the cluster velocities, as listed in Table 2. Data for passing frequencies were obtained by sampling 60 s of video data at 30 Hz in each viewing port. In analyzing the videotape, each 60 s sample was subdivided into about 10 sets; the average passing frequency for each of these 5–6 s sets was measured, with roughly 20–30 clusters appearing in each set, and then that group of 10 was averaged to yield an overall average. Subdividing the 60 s sample into a number of sets allows for the estimation of statistical confidence limits on the group average; this was typically found to be about $\pm 10\%$ for 90% confidence limits. Furthermore, the visual analysis of a sample was determined to be repeatable within about 5%, so that the total uncertainty on a given average passing frequency is about $\pm 15\%$. By using the velocity history of the clusters to convert the abscissa from distance to time, we introduce the uncertainty error associated with the velocity measurements (roughly $\pm 30\%$). Using a r.m.s. method for combining uncertainties [17], the total uncertainty in the measurement of the contact times is about $\pm 35\%$.

Figure 6 shows the passing frequency function for one of the operating conditions, the shape of which is typical of all of the operating conditions. Note that the type of curve that fits the passing frequencies best is an exponential function. Since the shedding function is the negative of the derivative of the passing

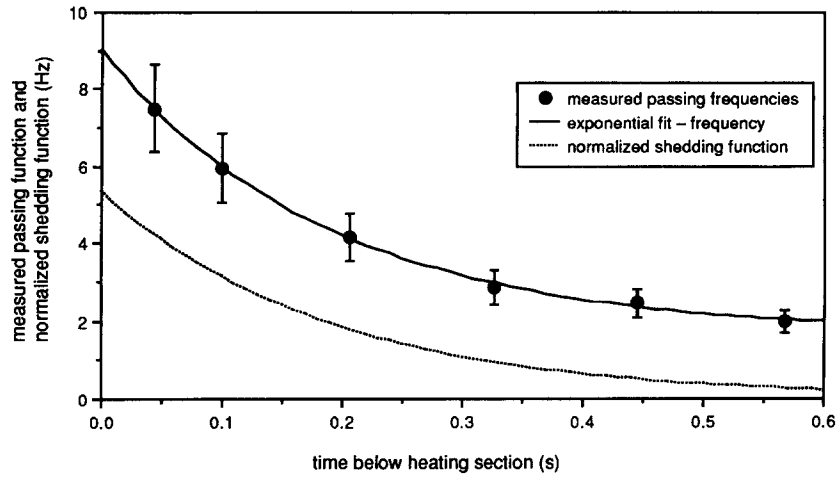

Fig. 6. Typical measured passing frequencies of clusters and exponential fit (from Case 5).

frequency, the shedding function will also have an exponential shape with the same time constant. If the shedding function is normalized such that the area under its curve is unity, then the shedding function is equivalent to the probability that a cluster travels a certain time after heating, as discussed previously. This normalized shedding function is also shown with the measurements in Fig. 6.

An exponential probability function, like the normalized shedding function that we can calculate from fitting the measurements of passing frequencies, is defined by:

$$m(\tau) = \frac{1}{\tau_{avg}} \cdot \exp\left(-\frac{\tau}{\tau_{avg}}\right) \tag{5}$$

where τ is the random variable and the average value is simply τ_{avg}. Since exponential functions fit the data best, τ_{avg} for each of the cases is simply the decay constant resulting from fitting an equation similar to equation (5) to the frequency functions; these values are given in Table 4. A probabilistic analysis [18] shows that the average total contact time, including the unobserved cluster–wall contact prior to heating, is simply double the average measured after heating, or $t_{avg} = 2 \cdot \tau_{avg}$. It can also be shown by the same analysis that the distribution of contact times for a particular case is described by a gamma probability function as follows:

$$p(t) = \frac{t}{\tau_{avg}^2} \cdot \exp\left(-\frac{t}{\tau_{avg}}\right). \tag{6}$$

Gamma probability functions have a parameter n associated with them; in this case, the parameter $n = 2$ [19].

Cluster–wall contact times—discussion

In concluding the analysis of the contact-time data, we present Fig. 7(a–c). These show how the total cluster–wall contact times vary with the superficial velocity of the gas, the solid recycle rate, and the average local cross-sectional solid concentration. For all three parameters, a slight downward trend is apparent, but it is difficult to confirm the existence of these trends as they fall within the range of experimental uncertainty. Since these are the only measurements of cluster–wall contact times, it is impossible to gather other data for comparison. Without additional data, we cannot confidently generalize the results and postulate mechanisms that govern the cluster–wall interaction.

Table 4. Measurements of cluster–wall contact times

Case number	u_o [m s^{-1}]	G_s [kg m^{-2} s]	Average time below heating section [s]	Average total contact time [s]
1	2.3	9.3	0.24	0.49
2	2.8	11	0.19	0.37
3	2.8	19	0.22	0.45
4	2.7	30	0.19	0.37
5	3.3	18	0.19	0.37
6	3.3	28	0.21	0.42
7	3.6	25	0.19	0.38
8	3.6	34	0.17	0.33

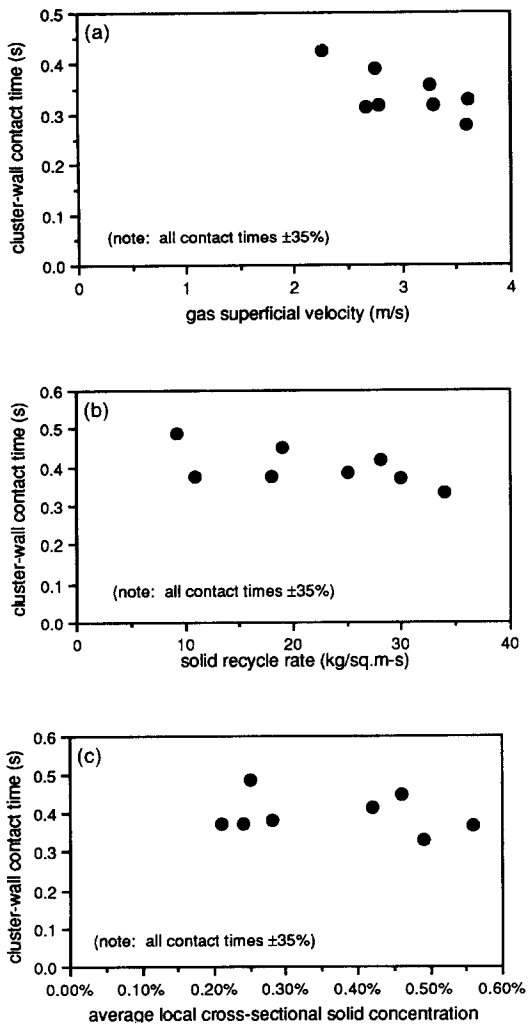

Fig. 7(a). Cluster–wall contact time vs gas velocity. (b) Cluster–wall contact time vs solid recycle rate. (c) Cluster–wall contact time vs solid concentration.

THE EFFECTS OF CLUSTER MOTION ON PARTICLE CONVECTION

Cluster acceleration

As discussed previously, the fact that the clusters do not travel at a constant velocity has the potential to affect conventional notions surrounding heat transfer by particle convection. When looking for a contact time to use in equation (1), it is easiest to assume that t is equal to some travel length divided by some velocity. However, the results presented here indicate that there may not be one single velocity for the flow of clusters at the wall. In this analysis, we will consider this problem using the cluster-acceleration model presented in equation (3), since it is the one that most clearly resembles the measured velocity histories in Fig. 5(a).

In theory, it is nice to deal with the concept of t, the contact time of a cluster with the wall of a CFB, as in equation (1). In practice, however, it is inconvenient to deal with temporal coordinates, since it is impractical and perhaps impossible to rescale the physical dimensions of a CFB relative to each cluster. Fang *et al.* [12] derived the following formula for calculating a cluster-averaged local particle-convective heat transfer coefficient:

$$h(x) = \frac{\int_{-x_0}^{0} h_t\left(\frac{x}{u_c}\right)\int_{x-x'}^{\infty} p(s)\,\mathrm{d}s\,\mathrm{d}x'}{\int_{-x_0}^{x}\int_{x-x'}^{\infty} p(s)\,\mathrm{d}s\,\mathrm{d}x'} + \frac{\int_{0}^{x} h_t\left(\frac{x-x'}{u_c}\right)\int_{x-x'}^{\infty} p(s)\,\mathrm{d}s\,\mathrm{d}x'}{\int_{-x_0}^{x}\int_{x-x'}^{\infty} p(s)\,\mathrm{d}s\,\mathrm{d}x'} \tag{7}$$

where x_0 is the adiabatic starting length, and the function $h_t(t)$ is given by:

$$h_t(t) = \left(R_{\text{contact}} + \sqrt{\frac{\pi t}{(k\rho c)_{\text{cluster}}}}\right)^{-1}. \tag{8}$$

Fang *et al.* nondimensionalized their results by defining $Nu(x) = h(x) \cdot R_{\text{contact}}$ and a parameter K, which is a function of cluster properties, and they were able to match measured heat transfer data from Wu *et al.* [20] reasonably well. This method relied on two assumptions: one was that there was a gamma probability distribution for cluster contact times, which we have verified experimentally; the other was that the contact time can be replaced by a characteristic length and velocity, and we have shown that the use of a single velocity may be incorrect. Their analysis has proven to be quite useful, however, as it is the first transformation of the time-dependent and cluster-oriented particle convection model to real spatial coordinates.

We can modify Fang's analysis to account for cluster acceleration by transforming the amount of time traveled into a function of the distance traveled; this relationship will not be linear because of the acceleration of the clusters. By assuming that equation (3) represents the velocity history of the clusters, we can find the function $x(t)$ since $u(t) = \mathrm{d}x/\mathrm{d}t$. Therefore, we can theoretically also find the function $t(x)$, although this is more difficult. Before continuing, we will nondimensionalize the problem by defining a dimensionless distance, ζ, and a dimensionless time, η:

$$\zeta = \frac{xg}{u_c^2}; \quad \eta = \frac{gt}{u_c} \tag{9}$$

where u_c represents the terminal velocity of the clusters. With these definitions, the solution for $\zeta(\eta)$, or the dimensionless result of integrating equation (3) is:

$$\zeta = \eta - [1 - \exp(-\eta)]. \tag{10}$$

By inspection of equation (10), a direct solution for the function $\eta(\zeta)$ is not possible; however, using expansion approximations and curve fitting, we can arrive at the following piece-wise definition for the function $\eta(\zeta)$, for which the maximum deviation from equation (10) can be shown to be 5%:

$$\eta = \begin{Bmatrix} \sqrt{2\zeta}, & \leqslant 0.05 \\ 1.82 \cdot \zeta^{0.58}, & 0.05 < \zeta < 1.25 \\ \zeta + 1, & \geqslant 1.25 \end{Bmatrix}. \tag{11}$$

With equation (11), we can find $Nu(\zeta)$—the dimensionless heat transfer coefficient as a function of the dimensionless distance along the wall by reformulating equation (7) as follows:

$$Nu(\zeta) = \frac{\displaystyle\int_{-\zeta_0}^{0} Nu_t(\eta(\zeta - \zeta') - \eta(-\zeta')) \int_{\eta(\zeta-\zeta')}^{\infty} p(\eta)\, d\eta\, d\zeta'}{\displaystyle\int_{-\zeta_0}^{\zeta} \int_{\eta(\zeta-\zeta')}^{\infty} p(\eta)\, d\eta\, d\zeta'} + \frac{\displaystyle\int_{0}^{\zeta} Nu_t(\eta(\zeta - \zeta')) \int_{\eta(\zeta-\zeta')}^{\infty} p(\eta)\, d\eta\, d\zeta'}{\displaystyle\int_{-\zeta_0}^{\zeta} \int_{\eta(\zeta-\zeta')}^{\infty} p(\eta)\, d\eta\, d\zeta'} \tag{12}$$

where $Nu_t(\eta(\zeta))$ represents the particle-convective Nusselt number as a function of time, which is a function of distance. In addition, the following definitions hold:

$$Nu_t(\eta) = \left(1 + K \cdot \sqrt{\frac{\eta}{\eta_{avg}}}\right)^{-1},$$

$$K = \frac{1}{R_{contact}} \cdot \sqrt{\frac{\pi u_c \eta_{avg}}{g(k\rho c)_{cluster}}} \tag{13}$$

and $p(\eta)$ is the gamma probability distribution described in equation (6). The only substantial modification to the analysis of Fang *et al.* [12] is that now we calculate the particle-convective heat transfer based on time as a nonlinear function of distance, the nonlinearity having been introduced as a result of cluster acceleration.

With equation (12), there are now three parameters that can be varied: η_{avg}, the dimensionless average contact time; K, the cluster-property parameter; and ζ_0, the adiabatic starting length. Based on conditions typically found in CFBs, as discussed previously, these parameters have values of $0 < n_{avg} < 100$ and $1 < K < 50$; ζ_0 depends on the specific design. The solutions for $Nu(\zeta)$ for two values of η_{avg} are shown in Fig. 8 along with the solutions using Fang's analysis; the modifications to Fang's analysis have little to no effect on $Nu(\zeta)$ for variations in K and ζ_0 for a given value of η_{avg}. As can be seen in Fig. 8, there can be significant error in assuming that the clusters travel at a constant velocity when the average contact time is relatively low. Fang's analysis will theoretically overpredict the cluster contribution to local heat transfer rates by about 50% if the average cluster–wall contact times are short enough. This result is supported by the fact that the nonlinearity in the distance–time relationship is greatest at small times (i.e. small values of η_{avg}). For the results presented here, $\eta_{avg} \approx 3$, so that the effect of cluster acceleration on heat transfer cannot be neglected.

The average contact time and the distribution of contact times

Prior to the analysis developed by Fang *et al.*, it was usually assumed that the particle-convective heat transfer rate would decrease monotonically as the length of the heat transfer surface increased. At some point on the surface, however, the probabilistic con-

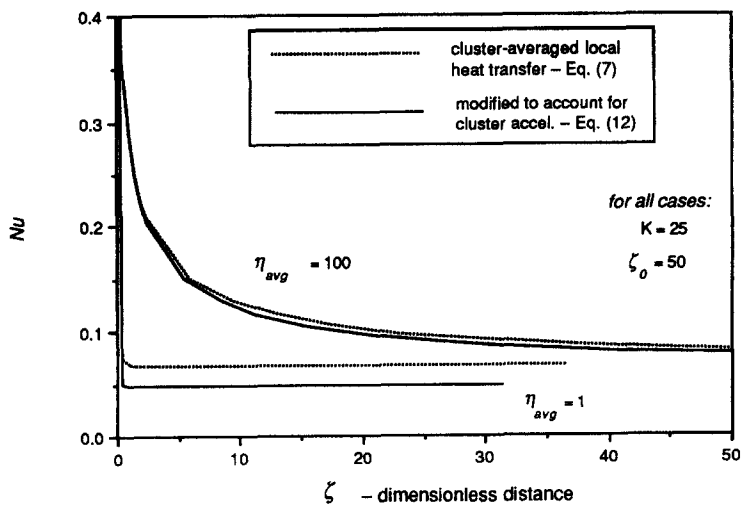

Fig. 8. Comparison of Nu predictions from equations (12) and (7).

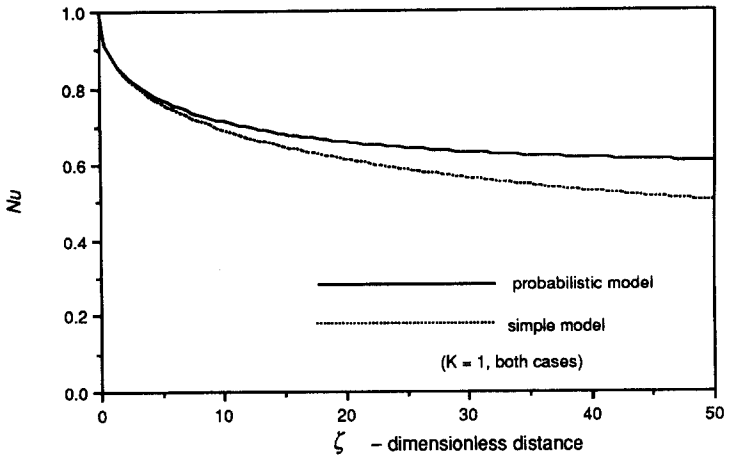

Fig. 9. $Nu(Z)$ compared to simplistic model, showing development region.

tact model predicts a departure from the simplistic model as the shedding and deposition of clusters becomes 'balanced' or 'developed'. Fang *et al.* showed that this model matched actual measurements. When the shedding and deposition processes become developed, the heat transfer coefficient approaches an asymptotic value, or a 'fully-developed' rate of particle-convective heat transfer, rather than continuing to decrease. This behavior is depicted in Fig. 9, where $K = 1$ is selected as a typical value expected (thermal development is reached more quickly for lower values of K since a low value of K implies a low average contact time or a relatively high contact resistance for a given cluster).

The 'fully-developed' particle-convective heat transfer coefficient can be obtained by modifying the simplistic particle-convection model. For a given jth cluster, the time-averaged heat transfer coefficient is:

$$h_j = \sqrt{\frac{4(k\rho c)_{\text{cluster}}}{\pi t_j}}. \tag{14}$$

For this cluster, the total energy transferred is given by:

$$e_j = (h_j \Delta T) \cdot t_j = \text{constant} \cdot \sqrt{t_j} \tag{15}$$

so that for a population of clusters, the average energy transferred is given by:

$$\bar{e}_j = \text{constant} \cdot \int_0^\infty t^{1/2} p(t)\, \mathrm{d}t. \tag{16}$$

Dividing by the average contact time per cluster, then, we can find the time- and cluster-averaged heat transfer coefficient for a population of clusters after reaching the development point:

$$h_\infty = \sqrt{\frac{4(k\rho c)_{\text{cluster}}}{\pi}} \cdot \left[\frac{\int_0^\infty t^{1/2} p(t)\, \mathrm{d}t}{\int_0^\infty t p(t)\, \mathrm{d}t} \right] \tag{17}$$

where we assumed that all clusters have the same properties. Since h_∞ is the 'fully-developed' cluster heat transfer coefficient, we can define t_∞ to be the time value appropriate for calculating h_∞:

$$h_\infty = \sqrt{\frac{4(k\rho c)_{\text{cluster}}}{\pi t_\infty}} \tag{18}$$

such that:

$$t_\infty = \left[\frac{\int_0^\infty t p(t)\, \mathrm{d}t}{\int_0^\infty t^{1/2} p(t)\, \mathrm{d}t} \right]^2. \tag{19}$$

To obtain the 'fully-developed' particle-convective heat transfer coefficient, $1/h_\infty$ is combined in series with R_{contact}, as in equation (1). Furthermore, for a gamma probability distribution with $n = 2$, it can be shown that t_∞ is related to the average contact time by:

$$t_\infty = \frac{64}{18\pi} \cdot t_{\text{avg}} = 1.13 \cdot t_{\text{avg}} \tag{20}$$

where the correction to t_{avg} is required to account for the effect of the distribution of contact times on the functional relation $h \approx 1/\sqrt{t}$. Therefore, the simplifications in equations (18) and (20) allow one to bypass the complex probabilistic model of equations (7) or (12) in order to calculate the local heat transfer coefficient relatively far along a given surface; this can be shown to work reasonably well for the data of Wu *et al.* [20].

CONCLUSIONS

In this paper, we have presented some new and unique hydrodynamic data that can be used to understand heat transfer at the walls of CFBs. In a cold scale-model CFB, we have found the following:

- a new experimental technique has been developed that can be used to measure the velocity, acceleration and contact times of clusters at the wall of a CFB;
- the terminal velocities of clusters at the wall of a CFB, for the given bed geometry and bed material, are about 1.2 m s^{-1} and are independent of operating conditions, similar to other observations;
- the clusters accelerate as if in gravitational free fall, verifying a previously postulated model, and the clusters appear to approach the terminal velocity due to a drag force that is linearly proportional to the velocity;
- the acceleration of clusters cannot necessarily be ignored when calculating heat transfer based on the particle-convective model, especially if the average contact time is short; ignoring this effect can result in the overprediction of the cluster contribution to heat transfer rates;
- the contact times of clusters with the smooth, plane wall of a CFB, for a given bed geometry and bed material, are between 0.35 and 0.50 s, with some variation observed with operating conditions;
- the measurements of contact times follow a probability distribution known as the gamma distribution, where the defining parameter is $n = 2$;
- the probabilistic contact behavior gives rise to a region in which the particle-convective heat transfer is developing, such that beyond this region the dependence on t is eliminated, resulting in a parameter t_∞ that can be defined to calculate the cluster contribution to heat transfer in the 'fully-developed' region.

Future studies are planned in which the TIV technique will be used to examine the influence of particle properties and wall geometry (e.g. water walls, horizontal riblets) on the cluster–wall interaction.

Acknowledgements—This work was sponsored by the National Science Foundation. The authors are grateful to MIT/Lincoln Laboratories and the Welding Laboratory at MIT for the use of their infrared cameras, and to the Fluid Mechanics Laboratory at MIT for the use of their VCR. The authors also acknowledge the contributions of Sushil Panta to this work.

REFERENCES

1. Ishii, H., Nakajima, T. and Horio, M., The clustering annular flow model of circulating fluidized beds. *Journal of Chemical Engineering of Japan*, 1989, **22,** 484–490.
2. Soong, C. H., Tuzla, K. and Chen, J. C., Identification of particle clusters in circulating fluidized beds. In *Circulating Fluidized Bed Technology IV*, ed. A. Avidan. American Institute of Chemical Engineers, 1993, pp. 615–620.
3. Rhodes, M., Mineo, H. and Hirama, T., Particle motion at the wall of a circulating fluidized bed. *Powder Technology*, 1992, **70,** 207–214.
4. Lim, K. S., Zhou, J., Finley, C., Grace, J. R., Lim, C. J. and Brereton, C. M. H., Cluster descending velocity at the wall of circulating fluidized bed risers. *5th International Conference on Circulating Fluidized Beds*, Beijing, People's Republic of China, May 1996.
5. Lints, M. C. and Glicksman, L. R., Parameters governing particle-to-wall heat transfer in a circulating fluidized bed. In *Circulating Fluidized Bed Technology IV*, ed. A. Avidan. American Institute of Chemical Engineers, 1993, pp. 297–304.
6. Wang, T., Lin, Z. J., Zhu, C. M., Liu, D. C. and Saxena, S. C., Particle velocity measurements in a circulating fluidized bed. *AIChE Journal*, 1993, **39,** 1406–1410.
7. Subbarao, D. and Basu, P., A model for heat transfer in circulating fluidized beds. *International Journal of Heat and Mass Transfer*, 1986, **29,** 487–489.
8. Mickley, H. S. and Fairbanks, D. F., Mechanism of heat transfer to fluidized beds. *AIChE Journal*, 1955, **1,** 374–384.
9. Baskakov, A. P., The mechanism of heat transfer between a fluidized bed and a surface. *International Chemical Engineering*, 1964, **4,** 320–324.
10. Gelperin, N. I. and Einstein, V. G., Heat transfer in fluidized beds. In *Fluidization*, ed. J. F. Davidson and D. Harrison, Chapter 10. Academic Press, New York, 1971.
11. Wu, R. L., Lim, C. J., Grace, J. R. and Brereton, C. M. H., Instantaneous local heat transfer and hydrodynamics in a circulating fluidized beds. *International Journal of Heat and Mass Transfer*, 1991, **34,** 2019–2027.
12. Fang, Z. H., Grace, J. R. and Lim, C. J., Local particle-convective heat transfer along surfaces in circulating fluidized beds. *International Journal of Heat and Mass Transfer*, 1995, **38,** 1217–1224.
13. Glicksman, L. R., Circulating fluidized bed heat transfer. In *Circulating Fluidized Bed Technology II*, ed. P. Basu and J. F. Large. Pergamon Press, Oxford, 1988, pp. 13–30.
14. Westphalen, D., Scaling and lateral solid mixing in circulating fluidized beds. Ph.D. thesis, Massachusetts Institute of Technology, Cambridge, MA, 1993.
15. Glicksman, L. R., Hyre, M. and Woloshun, K., Simplified scaling relationships for fluidized beds. *Powder Technology*, 1993, **77,** 177–199.
16. Lints, M. C., Particle-to-wall heat transfer in circulating fluidized beds. Sc.D. thesis, Massachusetts Institute of Technology, Cambridge, MA, 1992.
17. Beckwith, T. G., Marangoni, R. D. and Lienhard V., J. H., *Mechanical Measurements*, 5th edn, Chapter 3. Addison-Wesley, Reading, MA, 1993.
18. Panta, S. B., A probabilistic analysis for the interpretation of flow-visualization data at the wall of a circulating fluidized bed. B.S. thesis, Massachusetts Institute of Technology, Cambridge, MA, 1996.
19. Lapin, L. L., *Probability and Statistics for Modern Engineering*, 1st edn, Chapter 4. Brooks/Cole, Monterey, CA, 1983.
20. Wu, R. L., Grace, J. R., Lim, C. J. and Brereton, C. M. H., Suspension-to-surface heat transfer in a circulating-fluidized-bed combustor. *AIChE Journal*, 1989, **35,** 1685–1691.